SIAM J. APPL. MATH.
Vol. 65, No. 6, pp. 2067–2092

STIMULUS-LOCKED TRAVELING WAVES AND BREATHERS IN AN EXCITATORY NEURAL NETWORK*

STEFANOS E. FOLIAS† AND PAUL C. BRESSLOFF*

Abstract. We analyze the existence and stability of stimulus-locked traveling waves in a one-dimensional synaptically coupled excitatory neural network. The network is modeled in terms of a nonlocal integro-differential equation, in which the integral kernel represents the spatial distribution of synaptic weights, and the output firing rate of a neuron is taken to be a Heaviside function of activity. Given an inhomogeneous moving input of amplitude I_0 and velocity v, we derive conditions for the existence of stimulus-locked waves by working in the moving frame of the input. We use this to construct existence tongues in (v, I_0)-parameter space whose tips at $I_0 = 0$ correspond to the intrinsic waves of the homogeneous network. We then determine the linear stability of stimulus-locked waves within the tongues by constructing the associated Evans function and numerically calculating its zeros as a function of network parameters. We show that, as the input amplitude is reduced, a stimulus-locked wave within the tongue of an unstable intrinsic wave can undergo a Hopf bifurcation, leading to the emergence of either a traveling breather or a traveling pulse emitter.

Key words. traveling waves, traveling breathers, inhomogeneous neural media

AMS subject classification. 92C20

DOI. 10.1137/040615171

1. Introduction.

Understanding the conditions under which traveling waves of activity can propagate in cortical neural tissue is becoming an increasingly active area of research. Experimentally, these waves can be induced by a brief electrical stimulation of a disinhibited in vitro cortical slice [7, 14, 39, 29, 30]. The underlying mechanism for the propagation of such waves appears to be synaptic in origin rather than diffusive, with action potentials traveling along the axons of individual neurons. Axonal waves are modeled in terms of reaction diffusion equations based on either the four-variable Hodgkin–Huxley equations [20] or the reduced two-variable FitzHugh–Nagumo equations [12]. On the other hand, synaptic waves are typically modeled in terms of nonlocal integro-differential equations of the form [27]

$$\begin{aligned} \tau \frac{\partial u(x,t)}{\partial t} &= -u(x,t) + \int_{-\infty}^{\infty} w(x|x') f(u(x',t)) dx' - \beta q(x,t) + I(x,t), \\ \frac{1}{\epsilon} \frac{\partial q(x,t)}{\partial t} &= -q(x,t) + u(x,t), \end{aligned} \tag{1.1}$$

where τ is a membrane or synaptic time constant, $u(x,t)$ is a neural field that represents the local activity of a population of excitatory neurons at position $x \in \mathbb{R}$, $I(x,t)$ is an external input current, $f(u)$ denotes the output firing rate function, and $w(x|x')$ is the strength of connections from neurons at x' to neurons at x. The neural field $q(x,t)$ represents some form of local negative feedback mechanism such as spike frequency adaptation or synaptic depression, with β, ε determining the relative strength and rate of feedback. This form of inhibitory feedback is distinct from nonlocal synaptic inhibition, which tends to favor the formation of stationary bumps of

*Received by the editors September 15, 2004; accepted for publication (in revised form) February 24, 2005; published electronically August 9, 2005.
http://www.siam.org/journals/siap/65-6/61517.html
†Department of Mathematics, University of Utah, 155 S 1400 E, Salt Lake City, UT 84112 (sfolias@math.utah.edu, bressloff@math.utah.edu).

activity rather than traveling waves [38, 1, 28]. The nonlinear function f is typically taken to be a sigmoid function $f(u) = 1/(1 + \mathrm{e}^{-\gamma(u-\kappa)})$ with gain γ and threshold κ. Since there is strong vertical coupling between cortical layers, it is possible to treat a thin vertical cortical slice as an effective one-dimensional medium. Analysis of the model provides valuable information regarding how the speed of a traveling wave, which is relatively straightforward to measure experimentally, depends on various features of the underlying neural tissue [27]. Indeed, one prediction of the model, concerning how the speed of the wave depends on the firing threshold of the neurons, has recently been confirmed experimentally in disinhibited rat cortical slices [32]. External electric fields are used to modulate the threshold and thus control wave propagation.

One of the common assumptions in the analysis of traveling wave solutions of (1.1) is that the system is spatially homogeneous, that is, that the external input $I(x,t)$ is independent of both x and t and the synaptic weights depend only on the distance between presynaptic and postsynaptic cells, $w(x|x') = w(x - x')$. The existence of traveling waves can then be established for a class of positive, bounded weight distributions $w(x)$ that includes the exponential function $(2d)^{-1}\mathrm{e}^{-x/d}$, where d determines the range of synaptic coupling. For appropriate choices of network parameters, one finds that a single right- or left-moving traveling front exists in the absence of any feedback [4, 9, 21], whereas a pair of right- or left-moving traveling pulses exists when there is significant feedback [27]; numerically it is found that the faster pulse is stable, whereas the slower pulse is unstable. Following the original work of Amari [1], exact traveling wave solutions can be constructed by taking the high gain limit $\gamma \to \infty$, for which $f(u) = H(u - \kappa)$, where H is the Heaviside step function; that is, $H(u) = 1$ if $u \geq 0$ and $H(u) = 0$ if $u < 0$. The stability of traveling wave solutions of (1.1) in the case of a Heaviside firing rate function has recently been analyzed by Zhang [42, 43] using an Evans function approach. This is a technique for analyzing wave stability in unbounded domains that was originally developed within the context of reaction diffusion equations describing the axonal propagation of action potentials [10, 11, 22]. The basic idea is to linearize the full nonlinear equations about the traveling wave solution and to construct a complex analytic function known as the Evans function, whose zeros correspond to the point spectrum of the associated linear operator. Having established that the essential spectrum lies in the left-half complex plane, the wave is linearly stable if no eigenvalues have a positive real part and the zero eigenvalue is simple; the existence of the latter reflects the translation invariance of the system. Evans functions have now been applied to a variety of dissipative and Hamiltonian PDE systems [35], as well as a number of nonlocal integrodifferential equations [42, 43, 23, 34]. In the case of traveling wave solutions of (1.1), Zhang [42] derived an analytical expression for the Evans function using a variation of the parameters method to solve the inhomogeneous ordinary differential equation arising from linearization about the traveling wave solution. In the scalar case (zero feedback), the eigenvalues can be calculated explicitly and the associated front shown to be stable. On the other hand, for the full vector equation (1.1), it has been possible to prove stability of the fast traveling pulse only in the singular limit of slow feedback (small ε). However, one can still numerically evaluate the zeros of the Evans function outside this regime. This has been implemented by Coombes and Owen [8], who have extended the Evans function approach of Zhang [42] to a more general class of network models that incorporates discrete axonal delays and dendritic processing.

We have recently been interested in the effects of stationary inhomogeneous inputs on wave propagation and its failure in excitatory networks described by (1.1). As one

might expect intuitively, a sufficiently large variation in input blocks wave propagation (in one dimension) by spatially pinning the activity of the network. In particular, a step input or ramp results in a stationary front, whereas a local Gaussian input induces a stationary pulse. We have analyzed the stability of these stationary solutions for a Heaviside firing rate function, and shown how reducing the amplitude of the input can induce a Hopf bifurcation leading to the formation of a stable, spatially localized oscillatory solution, or *breather* [5, 13]. In the case of fronts, we have further shown that there is a critical level of negative feedback at which the homogeneous system undergoes a symmetry-breaking front bifurcation, whereby a stationary front loses stability and bifurcates into a pair of stable counterpropagating fronts. The front bifurcation acts as an organizing center for the formation of a breather in the presence of a weak input inhomogeneity [13]. Analogous results have been found for fronts [36, 18, 19, 2, 31] and pulses [33] in reaction diffusion systems. One of the potential difficulties in experimentally testing our predictions regarding input-induced coherent oscillations in cortical slices is that persistent currents tend to destroy the neurons. Although it might be possible to circumvent this problem using other forms of stimulation such as external electric fields [32], an alternative strategy is to consider the effects of moving stimuli. This is also more realistic from the perspective of the intact cortex, which is constantly being bombarded by nonstationary sensory inputs.

In this paper we extend the Evans function approach of Zhang [42] and our own previous work on stationary inhomogeneous inputs, in order to analyze the existence and stability of traveling waves locked to a moving input of constant speed v. In order to construct exact traveling wave solutions, we follow previous treatments [1, 27, 42] by considering a Heaviside firing rate function and a homogeneous weight distribution, for which (1.1) becomes

$$\tau \frac{\partial u(x,t)}{\partial t} = -u(x,t) - \beta q(x,t) + \int_{-\infty}^{\infty} w(x-x')H(u(x',t)-\kappa)dx' + I(x-vt),$$

$$\frac{1}{\epsilon}\frac{\partial q(x,t)}{\partial t} = -q(x,t) + u(x,t). \tag{1.2}$$

We assume throughout that $w(x)$ is a positive symmetric function that is monotonically decreasing on $[0,\infty)$ and satisfies the normalization condition $\int_{-\infty}^{\infty} w(x)dx < \infty$. The input is written as $I(x-vt) = I_0\,\chi(x-vt)$, with χ a fixed spatial profile that is either a bounded monotonically decreasing function in the case of fronts, or a unimodal Gaussian-like function in the case of pulses. The input amplitude I_0 and velocity v are treated as bifurcation parameters. Working in the moving frame of the input, we derive threshold-crossing conditions for the existence of a stimulus-locked wave, and use this to construct existence tongues in (v, I_0)-parameter space whose tips at $I_0 = 0$ correspond to the intrinsic waves of the homogeneous network, assuming that the latter exist. In the particular case of an exponential weight distribution, we show that there are two tongues in the positive v domain, corresponding to an unstable/stable pair of right-moving intrinsic waves. We determine the stability of the waves within these existence tongues by first constructing the Evans function for a general weight distribution w satisfying the properties listed below (1.2) and then numerically calculating the zeros of the Evans function for the exponential weight distribution. We show that as the input is reduced, a stimulus-locked wave within the tongue of the unstable intrinsic wave can undergo a Hopf bifurcation leading to the emergence of a traveling oscillatory wave. The latter takes the form of a breather or a pulse emitter in the moving frame of the stimulus. In the limit $v \to 0$ our results reduce to those previously obtained for stationary inputs [6, 13].

Note that analogous wave instabilities have been found in a scalar network with asymmetric lateral inhibition [40]. Such a network consists of a Mexican hat weight function $w_\circ$ that models short-range excitation and long-range inhibition, which is shifted asymmetrically from the center such that $w(x|x') = w_\circ(x - x' - s)$ for some fixed displacement s. This displacement introduces a form of directional selectivity, in which the network responds preferentially to stimuli moving in a particular direction, and has thus been suggested as a possible recurrent mechanism for the directional selectivity of neurons in visual cortex [37, 25]. Xie and Giese [40] have analyzed the existence and stability of stimulus-locked pulses in an asymmetric lateral inhibition network. They effectively construct the associated Evans function, although they do not identify it as such, and show how the pulse can destabilize when the stimulus velocity differs significantly from the natural velocity of unidirectional intrinsic waves; this instability generates a transition to a so-called lurching wave. Yet another neural system in which a traveling pulse can undergo a Hopf bifurcation leading to the formation of lurching waves is a synaptically coupled integrate-and-fire network with discrete axonal delays [15, 16]. Here a pulse consists of a single propagating spike, and the instability is due to fluctuations in the sequence of neuronal firing times, which start to grow at a critical value of the delay [3]. This example applies to intrinsic waves in a homogeneous network.

The structure of the paper is as follows. In order to illustrate the general approach, we begin by considering the simpler case of zero negative feedback ($\beta = 0$), for which (1.1) reduces to a scalar equation in u (section 2). The corresponding existence tongues for stimulus-locked fronts and their stability can be completely determined analytically. We next consider the existence of stimulus-locked pulses in the full vector system (1.1), numerically solving a set of nonlinear functional equations in order to construct the associated tongues (section 3). We then develop the linear stability analysis of stimulus-locked pulses in order to determine the stability of solutions within the tongues (section 4). Finally, we present numerical simulations illustrating the formation of traveling breathers and pulse emitters. Although we focus on traveling pulses rather than fronts in the case of the full system (1.1), it is straightforward to carry over our results to the case of stimulus-locked fronts, as briefly reported elsewhere [6]. Throughout the paper we work with dimensionless units. The fundamental time scale is taken to be the membrane time constant τ, which is assumed to be of the order 10 msec. The fundamental length scale is taken to be in the range d of synaptic coupling, which can vary from a few hundred micrometers to a few millimeters.

2. Stimulus-locked traveling fronts in a scalar equation. In this section we carry out a complete analysis of the existence and stability of stimulus-locked fronts in a scalar version of (1.2). As an illustrative example, we construct tongue diagrams for an exponential weight distribution, showing how the existence regions of fronts in the (v, I_0)-plane deform as the threshold κ is varied. We also establish that the fronts within the existence tongues are always stable.

2.1. Existence of stimulus-locked fronts. Consider

$$\frac{\partial u(x,t)}{\partial t} = -u(x,t) + \int_{-\infty}^{\infty} w(x-y)H(u(y,t)-\kappa)dy + I(x-vt), \tag{2.1}$$

where the input is taken to be a positive bounded monotonic function. We seek traveling front solutions of the form $u(x,t) = U(\xi)$, where $\xi = x - vt$ and

$$U(\xi) > \kappa, \quad \xi < \xi_0; \qquad U(\xi_0) = \kappa; \qquad U(\xi) < \kappa, \quad \xi > \xi_0,$$

for some $\xi_0 \in \mathbb{R}$. The wave of excitation is assumed to travel at the same velocity as the input, though the relative positions of the active region (above threshold) and the input may vary with respect to the velocity and the input strength. Thus, the active region is locked to the input but may precede or succeed the input in position. We take $U \in \mathcal{C}^1(\mathbb{R},\mathbb{R})$, where $\mathcal{C}^n(\mathbb{R},\mathbb{R})$ denotes the set of all n-times continuously differentiable functions $f : \mathbb{R} \longrightarrow \mathbb{R}$ that are bounded with respect to the sup norm. If $I_0 = 0$, then the system is translationally invariant and ξ_0 becomes a free parameter. In this case we refer to traveling waves as intrinsic or *natural* waves. The profile of the front is determined according to

$$-v\frac{dU(\xi)}{d\xi} = -U(\xi) + \int_{-\infty}^{\xi_0} w(\xi-\eta)d\eta + I(\xi). \tag{2.2}$$

Setting

$$W(\xi) = \int_{-\infty}^{\xi} w(\eta)d\eta,$$

we can integrate (2.2) over $[\xi,\infty)$ for $v > 0$ to obtain

$$U(\xi) = \frac{1}{v}\int_{\xi}^{\infty} e^{(\xi-\eta)/v} N_e(\eta;\xi_0)d\eta,$$

where

$$N_e(\xi;\xi_0) = 1 - W(\xi-\xi_0) + I(\xi).$$

We are assuming that w is normalized such that $\int_{-\infty}^{\infty} w(\eta)d\eta = 1$. Similarly, for $v < 0$ we integrate over $(-\infty,\xi]$ to find

$$U(\xi) = -\frac{1}{v}\int_{-\infty}^{\xi} e^{(\xi-\eta)/v} N_e(\eta;\xi_0)d\eta.$$

The threshold condition for the existence of a stimulus-locked front is $\kappa = U(\xi_0)$.

As a specific example, we consider a Heaviside input $I(\zeta) = I_0 H(-\zeta)$ and an exponential weight function

$$w(x) = \frac{1}{2d}e^{-|x|/d}, \tag{2.3}$$

with the length scale fixed by setting $d = 1$. The resulting threshold condition is

$$\kappa = \begin{cases} \dfrac{1}{2(1+v)} + \begin{cases} 0, & \xi_0 \geq 0, \\ I_0(1-e^{\xi_0/v}), & \xi_0 < 0, \end{cases} & v > 0, \\ \dfrac{1+2|v|}{2(1+|v|)} + \begin{cases} I_0 e^{\xi_0/v}, & \xi_0 > 0, \\ I_0, & \xi_0 \leq 0, \end{cases} & v < 0. \end{cases} \tag{2.4}$$

In the absence of an input ($I_0 = 0$), the threshold condition reduces to

$$\kappa = \begin{cases} \dfrac{1}{2(1+v_\circ)}, & v \geq 0, \\ \dfrac{1+2|v_\circ|}{2(1+|v_\circ|)}, & v < 0, \end{cases}$$

where $v_\circ$ is the natural speed of the wave. Solving for $v_\circ$ in terms of κ, we find that $v_\circ$ is a sigmoidal function of κ:

$$v_\circ(\kappa) = \begin{cases} \dfrac{\frac{1}{2}-\kappa}{\kappa}, & 0 < \kappa \leq \frac{1}{2}, \\ \dfrac{\frac{1}{2}-\kappa}{(\kappa-1)}, & \frac{1}{2} < \kappa < 1. \end{cases}$$

The homogeneous network supports a stationary natural front ($v_\circ = 0$) when $\kappa = \frac{1}{2}$, a front moving to the right for $0 < \kappa < \frac{1}{2}$, and front moving to the left for $\frac{1}{2} < \kappa < 1$. Moreover, $v_\circ \to \infty$ as $\kappa \to 0$ and $v_\circ \to -\infty$ as $\kappa \to 1$. It does not support a natural front when $\kappa > 1$, as any heteroclinic orbit joining the equilibrium $\{0, 1\}$ at infinity does not satisfy the threshold behavior used to define a traveling front solution. This recovers a result from [9].

We now analyze (2.4) for $I_0 > 0$ in order to determine the regions of the (v, I_0)-parameter subspace for which stimulus-locked waves exist. We first consider the case $v > 0$. For $\xi_0 \geq 0$ we have the threshold condition

$$\kappa = \frac{1}{2(1+v)},$$

and hence there are infinitely many waves parameterized by $\xi_0 \in [0, \infty)$, all of which travel with the natural speed $v = \frac{1-2\kappa}{2\kappa}$ for $0 < \kappa < \frac{1}{2}$. This degeneracy is a consequence of using the Heaviside input and would not occur if a continuous strictly monotonic input were used; however, the analysis is considerably more involved. For $\xi_0 < 0$ we have instead

$$\kappa = \frac{1}{2(1+v)} + I_0(1 - e^{\xi_0/v}).$$

As the right-hand side is monotonic in ξ_0, we can solve for ξ_0 as a function of v to obtain

$$\xi_0(v) = v \ln \left[1 - \frac{1}{I_0} \left(\kappa - \frac{1}{2(1+v)} \right) \right].$$

Since $\xi_0 < 0$ and $v > 0$, we see that solutions exist only if

$$0 < 1 - \frac{1}{I_0} \left(\kappa - \frac{1}{2(1+v)} \right) \leq 1$$

or, equivalently,

$$2(\kappa - I_0) \ < \ \frac{1}{1+v} \ \leq \ 2\kappa. \tag{2.5}$$

The right inequality of (2.5) implies that, if $\kappa < \frac{1}{2}$, then $v > v_\circ(\kappa)$, where $v_\circ$ is the corresponding natural velocity. Similarly, the left inequality implies that, if $I_0 < \kappa$, then $0 < v < v_1(\kappa - I_0)$, with $v_1(s) = \frac{1}{2s} - 1$. Hence, for $0 < \kappa \leq \frac{1}{2}$ we obtain the existence regions in the (v, I_0)-plane shown in Figure 2.1(a)–(b). The left boundary is given by $v = v_\circ(\kappa)$ and the right boundary by $v = v_1(\kappa - I_0)$. The two boundaries form a tongue that emerges from the natural speed $v_\circ(\kappa)$ at $I_0 = 0$.

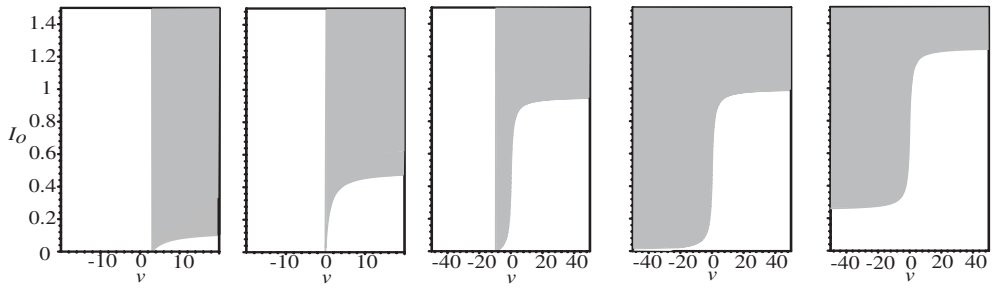

(a) $0 < \kappa < 1/2$ (b) $\kappa = 1/2$ (c) $1/2 < \kappa < 1$ (d) $\kappa = 1$ (e) $\kappa > 1$

FIG. 2.1. *Deformation of existence regions (gray) for stimulus-locked traveling fronts as* κ *varies in the scalar equation. Particular values of* κ *are as follows:* (a) $\kappa = 0.125$, (c) $\kappa = 0.95$, (e) $\kappa = 1.25$.

Now consider $v < 0$. For $\xi_0 < 0$ we have the threshold condition

$$\kappa = \frac{1 + 2|v|}{2(1 + |v|)} + I_0,$$

which implies

$$|v| = \frac{1 - 2(\kappa - I_0)}{2(\kappa - I_0 - 1)} \equiv v_2(\kappa - I_0).$$

Again we have an infinite family of waves corresponding to a single speed. Since $|v| \geq 0$, such solutions exist only for

$$\kappa - 1 \ < \ I_0 \ < \ \kappa - \frac{1}{2}.$$

On the other hand, for $\xi_0 \geq 0$ we have the threshold condition

$$\kappa = \frac{1 + 2|v|}{2(1 + |v|)} + I_0 e^{\xi_0/v}.$$

Monotonicity of the right-hand side again allows us to solve for $\xi_0(v)$ to find

$$\xi_0(v) = v \ln \left[\frac{1}{I_0} \left(\kappa - \frac{1 + 2|v|}{2(1 + |v|)} \right) \right],$$

and, since $v < 0$ and $\xi_0 \geq 0$, it follows that waves exist only for v satisfying

$$\kappa - I_0 \leq \frac{1 + 2|v|}{2(1 + |v|)} < \kappa. \tag{2.6}$$

The right inequality of (2.6) implies that if $\frac{1}{2} < \kappa < 1$, then $v_\circ(\kappa) < v < 0$. Thus, for $\frac{1}{2} < \kappa < 1$ we obtain the existence region shown in Figure 2.1(c); the left boundary is given by $v = v_0(\kappa)$ and the right boundary by $v = v_2(\kappa - I_0)$ for $v < 0$ and $v = v_1(\kappa - I_0)$ for $v > 0$. Again there is a tongue with tip at the natural speed. For $\kappa > 1$ the left boundary disappears, and one finds stimulus-locked waves only when $I_0 > \kappa - 1$, i.e., when there no longer exist natural waves. The left inequality of (2.6) implies that if $\frac{1}{2} < \kappa - I_0 < 1$, then $v < v_2(\kappa - I_0) < 0$, whereas if $\kappa - I_0 > 1$, then no solution exists. For all $\kappa > 1$ the region of existence is identical to that for $\kappa = 1$, though it is shifted vertically by $\kappa - 1$, as shown in Figure 2.1(d)–(e).

2.2. Stability of stimulus-locked fronts. Consider the evolution of small smooth perturbations $\bar{\varphi}$ of the stimulus-locked front solution U. Linearizing (2.1) about the wave, the perturbations evolve according to

$$\frac{\partial \bar{\varphi}}{\partial t} - v\frac{\partial \bar{\varphi}}{\partial \xi} + \bar{\varphi} = \int_{\mathbb{R}} w(\xi-\eta)H'(U(\eta)-\kappa)\bar{\varphi}(\eta)d\eta. \tag{2.7}$$

Separating variables, $\bar{\varphi}(\xi,t) = \varphi(\xi)e^{\lambda t}$, we find that $\varphi \in \mathcal{C}^1(\mathbb{R},\mathbb{C})$ satisfies the eigenvalue problem

$$(\mathcal{L}+\mathcal{N}_s)\,\varphi = \lambda\,\varphi, \tag{2.8}$$

where

$$\mathcal{L}\varphi = v\frac{\partial \varphi}{\partial \xi} - \varphi, \qquad \mathcal{N}_s\varphi\,(\xi) = \frac{w(\xi-\xi_0)}{|U'(\xi_0)|}\,\varphi(\xi_0). \tag{2.9}$$

We need to characterize the spectrum of the linear operator $\mathcal{L}+\mathcal{N}_s : \mathcal{C}^1(\mathbb{R},\mathbb{C}) \longrightarrow \mathcal{C}^0(\mathbb{R},\mathbb{C})$ in order to determine the linear stability of the traveling pulse. The following definitions concern linear operators $\mathcal{T} : \mathcal{D}(\mathcal{T}) \longrightarrow \mathcal{B}$, where $\mathcal{B}$ is a Banach space and the domain $\mathcal{D}(\mathcal{T})$ of $\mathcal{T}$ is dense in $\mathcal{B}$ [41]. In our case $\mathcal{D}(\mathcal{L}+\mathcal{N}_s) = \mathcal{C}^1(\mathbb{R},\mathbb{C})$, which is dense in $\mathcal{C}^0(\mathbb{R},\mathbb{C})$. λ is in the resolvent set ρ if $\lambda \in \mathbb{C}$ is such that $\mathcal{T}-\lambda$ has a range dense in $\mathcal{B}$ and a continuous inverse $(\mathcal{T}-\lambda)^{-1}$; otherwise λ is in the spectrum σ. We decompose the spectrum into the following disjoint sets: λ is an element of the point spectrum σ_p if $\mathcal{T}-\lambda$ is not invertible; λ is an element of the continuous spectrum σ_c if $\mathcal{T}-\lambda$ has an unbounded inverse with domain dense in $\mathcal{B}$; λ is an element of the residual spectrum σ_r if $\mathcal{T}-\lambda$ has an inverse (bounded or not) whose domain is not dense in $\mathcal{B}$. We refer to elements of the point spectrum as eigenvalues and the union of the continuous and residual spectra as the essential spectrum.

Regarding the essential spectrum, we mention that $\mathcal{N}_s$ is a compact linear operator. The consequence is that, since $\mathcal{N}_s$ is compact, the operators $\mathcal{L}+\mathcal{N}_s$ and $\mathcal{L}$ have the same essential spectra [24, 23]. To see that the operator is compact, we define $\mathcal{N}_s$ by the composition $\mathcal{TS}$, where

$$\mathcal{S}\,\varphi = \varphi(\xi_0), \qquad (\mathcal{T}\,z)(\xi) = \frac{w(\xi-\xi_0)}{|U'(\xi_0)|}z.$$

Since $\mathcal{S} : \mathcal{C}^1(\mathbb{R},\mathbb{C}) \longrightarrow \mathbb{C}$ has a finite-dimensional range, it is a compact linear operator. Moreover, since $\mathcal{T} : \mathbb{C} \longrightarrow \mathcal{C}^0(\mathbb{R},\mathbb{C})$ is a bounded linear operator, it follows that the composition $\mathcal{TS}$ is a compact linear operator.

Resolvent and the point spectrum. We seek to construct a bounded inverse by solving the inhomogeneous equation

$$(\mathcal{L}+\mathcal{N}_s-\lambda)\varphi = -f, \tag{2.10}$$

where $f \in \mathcal{C}^0(\mathbb{R},\mathbb{C})$, using a variation of parameters approach along the lines of Zhang [42]. We write (2.10) as

$$\frac{\partial}{\partial \xi}\Big(e^{-\left(\frac{1+\lambda}{v}\right)\xi}\,\varphi(\xi)\Big) = -\frac{1}{v}\,e^{-\left(\frac{1+\lambda}{v}\right)\xi}\,\Big(\mathcal{N}_s\varphi(\xi)+f(\xi)\Big). \tag{2.11}$$

For $\frac{\mathcal{R}e(\lambda)+1}{v} > 0$, integrating (2.11) over $[\xi,\infty)$ yields

$$\varphi(\xi) - \Lambda_+(\lambda;\xi)\,\varphi(\xi_0) \;=\; \mathcal{H}_f(\xi), \tag{2.12}$$

where

$$\Lambda_+(\lambda;\xi) = \frac{1}{v|U'(\xi_0)|}\int_\xi^\infty w(\eta-\xi_0)e^{\left(\frac{1+\lambda}{v}\right)(\xi-\eta)}d\eta,$$

$$\mathcal{H}_f(\xi) = \frac{1}{v}\int_\xi^\infty e^{\left(\frac{1+\lambda}{v}\right)(\xi-\eta)}f(\eta)d\eta.$$

Using the Hölder inequality, it can be shown that both $\Lambda_+(\lambda;\xi)$ and $\mathcal{H}_f(\xi)$ are bounded for all $\xi \in \mathbb{R}$ and $f \in \mathcal{C}^0(\mathbb{R},\mathbb{C})$. It is then seen from (2.12) that $\varphi(\xi)$ is determined by its restriction $\varphi(\xi_0)$, in which case we obtain

$$\left(1-\Lambda_+(\lambda;\xi_0)\right)\varphi(\xi_0) = \frac{1}{v}\int_{\xi_0}^\infty e^{\left(\frac{1+\lambda}{v}\right)(\xi-\eta)}f(\eta)d\eta.$$

This can be solved for $\varphi(\xi_0)$ and hence for $\varphi(\xi)$ if and only if

$$1-\Lambda_+(\lambda;\xi_0) \neq 0.$$

This results in a bounded inverse which is defined on all of $\mathcal{C}^0(\mathbb{R},\mathbb{C})$, and therefore all corresponding λ are in the resolvent set. On the other hand, we cannot invert the operator for λ such that

$$1-\Lambda_+(\lambda;\xi_0) = 0.$$

In this case

$$(\mathcal{L}+\mathcal{N}_s-\lambda)\varphi = 0 \tag{2.13}$$

has nontrivial solutions, indicating that λ is in the point spectrum. Moreover, if we define the function

$$\mathcal{E}_+(\lambda;\xi_0) = 1-\Lambda_+(\lambda;\xi_0), \qquad \frac{\mathcal{R}e(\lambda)+1}{v} > 0,$$

we see that eigenvalues form the zero set. Similarly for $\frac{\mathcal{R}e(\lambda)+1}{v} < 0$, integrating (2.11) over $(-\infty,\xi_0]$ yields a similar condition for the existence of eigenfunctions

$$1 = \Lambda_-(\lambda,\xi_0), \qquad \frac{\mathcal{R}e(\lambda)+1}{v} < 0,$$

where

$$\Lambda_-(\lambda;\xi) = -\frac{1}{v|U'(\xi_0)|}\int_{-\infty}^\xi w(\eta-\xi_0)e^{\left(\frac{1+\lambda}{v}\right)(\xi-\eta)}d\eta. \tag{2.14}$$

The Evans function is then defined as

$$\mathcal{E}(\lambda;\xi_0) = 1-\Lambda_\pm(\lambda;\xi_0), \qquad \frac{\mathcal{R}e(\lambda)+1}{v} \gtrless 0.$$

Essential spectrum. Since $\mathcal{N}_s$ does not contribute to the essential spectrum of $\mathcal{L}+\mathcal{N}_s$, we need only calculate the essential spectrum of the linear operator $\mathcal{L}$. The essential spectrum is the set of $\lambda = -1 + iv\rho$, where $\rho \in \mathbb{R}$. Since this has negative real part, the essential spectrum does not contribute to any wave instabilities. We demonstrate that, for these values of λ, there exist bounded functions for which the inverse operator $(\mathcal{L}-\lambda)^{-1}$ becomes unbounded, indicating that λ is a member of the continuous spectrum.

Suppose that $\lambda = -1 + iv\rho$, and consider the sequence of bounded functions [43]

$$\varphi_m(\xi) = (1 - e^{-\xi^2/2m^2})e^{i\rho\xi}, \qquad m \in \mathbb{N},$$

for which

$$\|\varphi_m\|_\infty = 1 \qquad \forall \ \ m \in \mathbb{N},\ \rho \in \mathbb{R}.$$

However,

$$(\mathcal{L}-\lambda)\varphi_m(\xi) = \frac{v}{m^2}\ \xi e^{-\xi^2/2m^2}\ e^{i\rho\xi},$$

which implies that

$$\left\|(\mathcal{L}-\lambda)\varphi_m\right\|_\infty = \frac{v}{m^2}\left\|\xi e^{-\xi^2/2m^2}\right\|_\infty \longrightarrow 0 \quad \text{as} \quad m \longrightarrow \infty.$$

Hence, $(\mathcal{L}-\lambda)^{-1}$ is unbounded, and the set of $\lambda = -1 + iv\rho$, where $\rho \in \mathbb{R}$, form the essential spectrum. The residual spectrum in this case is empty, though we shall see that the vector system does, in fact, have a nonempty residual spectrum.

Evans function for an exponential weight distribution. We now explicitly calculate the zeros of the Evans functions for a Heaviside input and exponential weight distribution. The region in the complex plane $\mathbf{D} = \{z \ : \ \mathcal{R}e(z) > -1\}$ is the domain of the Evans function $\mathcal{E}_+$, and we need only consider this region to determine the stability of the wave. For $v > 0$ and $\lambda \in \mathbf{D}$,

$$\begin{aligned}\mathcal{E}_+(\lambda,\xi_0) &= 1 - \frac{1}{v|U'(\xi_0)|}\int_{\xi_0}^{\infty} w(\eta-\xi_0)e^{\left(\frac{1+\lambda}{v}\right)(\xi_0-\eta)}d\eta \\ &= 1 - \frac{1}{2(1+\lambda+v)}\frac{1}{|U'(\xi_0)|},\end{aligned}$$

and similarly for $v < 0$ and $\lambda \in \mathbf{D}$,

$$\begin{aligned}\mathcal{E}_-(\lambda,\xi_0) &= 1 + \frac{1}{v|U'(\xi_0)|}\int_{-\infty}^{\xi_0} w(\eta-\xi_0)e^{\left(\frac{1+\lambda}{v}\right)(\xi_0-\eta)}d\eta \\ &= 1 + \frac{1}{2(1+\lambda+v)}\frac{1}{|U'(\xi_0)|}.\end{aligned}$$

Note that this recovers the Evans function obtained by Zhang [42] in the case of a homogeneous input. From this we can directly solve $\mathcal{E}_\pm(\lambda;\xi_0) = 0$ for λ:

$$\lambda = -(1+|v|) + \frac{1}{2|U'(\xi_0)|}, \qquad v \in \mathbb{R}, \tag{2.15}$$

with $U'(\xi_0)$ determined from (2.2),

$$U'(\xi_0) = \frac{1}{v}\left(U(\xi_0) - \int_{-\infty}^{\xi_0} w(\xi_0 - \eta)d\eta - I(\xi_0)\right)$$
$$= \frac{1}{v}\left(\kappa - \frac{1}{2} - I(\xi_0)\right)$$

and κ satisfying the self-consistency conditions (2.4).

In the case $I_0 = 0$ the eigenvalues are given by

$$\lambda = -(1 + |v|) + \frac{|v|}{2\left|\kappa - \frac{1}{2}\right|}, \qquad v \in \mathbb{R}, \tag{2.16}$$

where v is the natural wave speed. Substituting (2.4) into (2.16), we find that the only eigenvalue in $\mathbf{D}$ is the zero eigenvalue $\lambda = 0$. Moreover, it can be shown that the eigenvalue is simple [42] and hence that the natural front is linearly stable, modulo uniform translations.

In the case of an inhomogeneous input ($I_0 > 0$), we have to deal with each of the separate subdomains of the threshold conditions (2.4). First, for $v > 0,\ \xi_0 > 0$ we notice that $I(\xi_0) = 0$ and κ is identical to the case of a natural wave; hence, $\lambda = 0$ is the only eigenvalue in $\mathbf{D}$. If $v > 0,\ \xi_0 < 0$, substituting (2.4) for κ into (2.15) yields the eigenvalue

$$\lambda = -1 - v + \frac{v}{2|\kappa - \frac{1}{2} - I_0|}$$
$$= (1 + v)\left[-1 + \frac{v}{\left|v + 2(1 + v)I_0(1 - e^{\xi_0/v})\right|}\right].$$

Since $I_0(1 - e^{\xi_0/v}) > 0$ for all $v > 0,\ \xi_0 < 0,\ I_0 > 0$, it follows that $\lambda < 0$ and the corresponding front is always stable. On the other hand, if $v < 0$ and $\xi_0 < 0$, we find $\lambda = 0$, again indicating stability with respect to the degenerate family of waves corresponding to the boundary of the tongue. For $\xi_0 > 0$ we similarly calculate

$$\lambda = (1 + |v|)\left[-1 + \frac{|v|}{\left||v| + 2(1 + |v|)I_0 e^{\xi_0/v}\right|}\right].$$

Since $2(1 + |v|)I_0 e^{\xi_0/v} > 0$ for $v < 0,\ \xi_0 > 0,\ I_0 > 0$, it again follows that $\lambda < 0$ and the corresponding front is always stable.

3. Stimulus-locked traveling pulses in the vector system. In this section we construct stimulus-locked traveling pulse solutions of (1.2) in the case of a unimodal input moving with constant velocity v. We first derive the formal solution for a general weight distribution w, and then use this to construct existence tongues in the (v, I_0)-plane for an exponential weight distribution and a Gaussian input of amplitude I_0.

3.1. Existence of stimulus-locked pulses. Consider a traveling pulse that is generated by, and locked to, an inhomogeneous input I traveling with constant speed v. Such a wave has permanent or *stationary* form; i.e., it translates as a rigid structure. Define the traveling wave coordinates (ξ, t), where $\xi = x - vt$ and v is

the velocity associated with the input. A *stimulus-locked traveling pulse* is a pair of functions (U,Q), with $U,Q \in \mathcal{C}^1(\mathbb{R},\mathbb{R})$, which in traveling wave coordinates satisfy the conditions

$$\begin{aligned} &U(\xi_i)=\kappa, \qquad i=1,2; && U(\xi)\longrightarrow 0 \qquad \text{as } \xi\longrightarrow\pm\infty;\\ &U(\xi)>\kappa, \qquad \xi_1<\xi<\xi_2; && U(\xi) < \kappa, \qquad \text{otherwise,}\end{aligned}$$

with ξ_1,ξ_2 defining the points at which the activity U crosses threshold. Taking $u(x,t)=U(x-vt)$ and $q(x,t)=Q(x-vt)$, the profile of the pulse is governed by

$$\begin{aligned} -v\,U_\xi &= -U-\beta Q+\int_{\xi_1}^{\xi_2} w(\xi-\eta)d\eta + I(\xi),\\ -\frac{v}{\epsilon}\,Q_\xi &= -Q \;+\; U.\end{aligned}$$

In general, we take the excitatory weight function $w(x)$ to be nonnegative, continuous, symmetric in x, and monotonically decreasing in $|x|$. Let $\mathbf{s}=(U,Q)^T$ and W denote an antiderivative of w; we can rewrite the system more compactly as

$$\mathcal{L}\mathbf{s} \equiv \begin{pmatrix} vU_\xi - U - \beta Q \\ vQ_\xi + \epsilon U - \epsilon Q\end{pmatrix} = -\begin{pmatrix} N_e \\ 0\end{pmatrix}, \tag{3.1}$$

where

$$N_e(\xi) = W(\xi-\xi_1) - W(\xi-\xi_2) + I(\xi). \tag{3.2}$$

We use variation of parameters to solve this linear equation. The homogeneous problem $\mathcal{L}\mathbf{s}=\mathbf{0}$ has the two linearly independent solutions,

$$\mathbf{S}_+(\xi) = \begin{pmatrix} \beta \\ m_+ - 1\end{pmatrix}\exp(\mu_+\xi), \qquad \mathbf{S}_-(\xi) = \begin{pmatrix} \beta \\ m_- - 1\end{pmatrix}\exp(\mu_-\xi),$$

where

$$\mu_\pm = \frac{m_\pm}{v}, \qquad m_\pm = \frac{1}{2}\Big(1+\epsilon \pm \sqrt{(1-\epsilon)^2-4\epsilon\beta}\Big).$$

We set

$$\mathbf{s}(\xi) = \Big[\mathbf{S}_+\big|\mathbf{S}_-\Big]\begin{pmatrix} a(\xi)\\ b(\xi)\end{pmatrix},$$

where $a,b\in\mathcal{C}^1(\mathbb{R},\mathbb{R})$ and $[A|B]$ denotes the matrix whose first column is defined by the vector A and whose second column is defined by the vector B. Since $\mathcal{L}\mathbf{S}_\pm = 0$, (3.1) becomes

$$\Big[\mathbf{S}_+\big|\mathbf{S}_-\Big]\,\frac{\partial}{\partial\xi}\begin{pmatrix} a(\xi)\\ b(\xi)\end{pmatrix} = -\frac{1}{v}\begin{pmatrix} N_e(\xi)\\ 0\end{pmatrix}. \tag{3.3}$$

Since $[\mathbf{S}_+|\mathbf{S}_-]$ is invertible, we find

$$\frac{\partial}{\partial\xi}\begin{pmatrix} a(\xi)\\ b(\xi)\end{pmatrix} = -\frac{1}{v\beta(m_+-m_-)}\Big[\mathbf{Z}_+\big|\mathbf{Z}_-\Big]^T\begin{pmatrix} N_e(\xi)\\ 0\end{pmatrix},$$

where

$$\mathbf{Z}_+(\xi) = \begin{pmatrix} 1-m_- \\ \beta \end{pmatrix} \exp(-\mu_+\xi), \qquad \mathbf{Z}_-(\xi) = -\begin{pmatrix} 1-m_+ \\ \beta \end{pmatrix} \exp(-\mu_-\xi).$$

For $v > 0$, we integrate over $[\xi, \infty)$ to obtain

$$\begin{pmatrix} a(\xi) \\ b(\xi) \end{pmatrix} = \begin{pmatrix} a_\infty \\ b_\infty \end{pmatrix} + \frac{1}{v\beta(m_+ - m_-)} \int_\xi^\infty \Big[\mathbf{Z}_+ \big| \mathbf{Z}_-\Big]^T \begin{pmatrix} N_e(\eta) \\ 0 \end{pmatrix} d\eta,$$

where a_∞, b_∞ denote the values of $a(\xi), b(\xi)$ as $\xi \longrightarrow \infty$. Thus

(3.4)
$$\mathbf{s}(\xi) = \Big[\mathbf{S}_+ \big| \mathbf{S}_-\Big] \begin{pmatrix} a_\infty \\ b_\infty \end{pmatrix} + \frac{1}{v\beta(m_+ - m_-)} \Big[\mathbf{S}_+ \big| \mathbf{S}_-\Big] \int_\xi^\infty \Big[\mathbf{Z}_+ \big| \mathbf{Z}_-\Big]^T \begin{pmatrix} N_e(\eta) \\ 0 \end{pmatrix} d\eta.$$

Using the Hölder inequality and that $N_e \in \mathcal{C}^0(\mathbb{R}, \mathbb{R})$, it is straightforward to show that the integral term in (3.4) is bounded for all $\xi \in \mathbb{R}$; hence, a bounded solution $\mathbf{s}$ exists only if $a_\infty = b_\infty = 0$. The general stimulus-locked pulse is given by

$$\mathbf{s}(\xi) = \frac{1}{v\beta(m_+ - m_-)} \Big[\mathbf{S}_+ \big| \mathbf{S}_-\Big] \int_\xi^\infty \Big[\mathbf{Z}_+ \big| \mathbf{Z}_-\Big]^T \begin{pmatrix} N_e(\eta) \\ 0 \end{pmatrix} d\eta.$$

Furthermore, if we define the functions

$$\mathcal{M}_\pm(\xi) = \frac{1}{v(m_+ - m_-)} \int_\xi^\infty e^{\mu_\pm(\xi-\eta)} N_e(\eta) d\eta,$$

we can express the solution (U, Q) as follows:

$$U(\xi) = (1-m_-)\mathcal{M}_+(\xi) - (1-m_+)\mathcal{M}_-(\xi), \tag{3.5}$$

$$Q(\xi) = \beta^{-1}(m_+ - 1)(1-m_-)\big[\mathcal{M}_+(\xi) - \mathcal{M}_-(\xi)\big]. \tag{3.6}$$

Since $N_e(\xi)$ is dependent upon ξ_1, ξ_2, the threshold conditions $U(\xi_i) = \kappa$, where $i = 1, 2$ and $\xi_1 < \xi_2$, determine the relationship between the input strength I_0 and the position of the pulse relative to the input I. This provides the following consistency conditions for the existence of a stimulus-locked traveling pulse, which, we note, reduce to the case of natural waves for $I_0 = 0$:

$$\kappa = (1-m_-)\mathcal{M}_+(\xi_1) - (1-m_+)\mathcal{M}_-(\xi_1), \tag{3.7}$$

$$\kappa = (1-m_-)\mathcal{M}_+(\xi_2) - (1-m_+)\mathcal{M}_-(\xi_2). \tag{3.8}$$

3.2. Pulses for an exponential weight distribution. Consider, in particular, an exponential weight distribution given by (2.3) with $d = 1$ and a Gaussian input

$$I(x) = I_0\, e^{-(x/\sigma)^2}. \tag{3.9}$$

Existence conditions determined from (3.7) and (3.8) yield the following system of nonlinear equations that determines the relationship between the input parameters (v, I_0) and the threshold points (ξ_1, ξ_2):

$$\kappa = K(\xi_1 - \xi_2) + T_+(\xi_1) - T_-(\xi_1), \tag{3.10}$$

$$\kappa = J(\xi_1 - \xi_2) + T_+(\xi_2) - T_-(\xi_2), \tag{3.11}$$

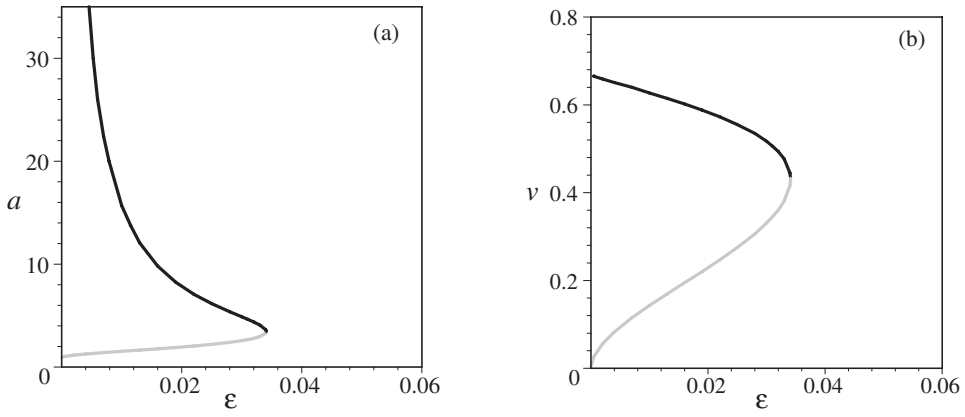

FIG. 3.1. *Bifurcation curves for the existence of natural traveling pulses ($I_0 = 0$) for the vector system* (1.2) *in* (a) *the (ϵ, a)-plane and* (b) *the (ϵ, v)-plane, illustrating that natural waves exist only for small ϵ. Here $a = \xi_2 - \xi_1$ denotes the width of a pulse. The stable branch (black), characterized by wide (large a), fast pulses, and the unstable branch (gray), characterized by narrow, slow pulses, annihilate in a saddle-node bifurcation at a critical value ϵ_c. In this case $\kappa = 0.3$, $\beta = 2.5$, and $\epsilon_c \approx 0.341$.*

where

$$K(\zeta) = K_0 + K_1 e^{\zeta} - K_+ e^{\mu_+ \zeta} + K_- e^{\mu_- \zeta}, \qquad J(\zeta) = \frac{v+\epsilon}{2(v+m_+)(v+m_-)}\Big(1 - e^{\zeta}\Big),$$

$$K_1 = \frac{1}{2}\frac{v-\epsilon}{(v-m_+)(v-m_-)}, \qquad K_\pm = \frac{v^2(1-m_\mp)}{m_\pm(v^2 - {m_\pm}^2)(m_+ - m_-)},$$

$$K_0 = \left(\frac{(1-m_-)(2v+m_+)}{2m_+(v+m_+)(m_+-m_-)}\right) - \left(\frac{(1-m_+)(2v+m_-)}{2m_-(v+m_-)(m_+-m_-)}\right),$$

$$T_\pm(\zeta) = \frac{\sqrt{\pi}\ \sigma I_0}{2\ v}\ \left(\frac{1-m_\mp}{m_+ - m_-}\right) \exp\left(\frac{(\mu_\pm \sigma)^2}{4} + \mu_\pm \zeta\right) \mathbf{erfc}\left(\frac{\zeta}{\sigma} + \frac{\mu_\pm \sigma}{2}\right),$$

and $\mathbf{erfc}(z)$ denotes the complementary Error function.

Natural traveling pulses ($I_0 = 0$). Numerically solving (3.10) and (3.11) for $I_0 = 0$, we find that for sufficiently small ϵ there exists a pair of traveling pulses arising from a saddle-node bifurcation. Numerical simulations suggest that the larger and faster pulse is stable while the smaller slower pulse is unstable and acts as a separatrix between the fast pulse and the rest state [27]. Zhang's analysis has shown the fast pulse to be stable in the singular limit $\epsilon \longrightarrow 0$ [42]. In Figure 3.1 we present bifurcation diagrams using ϵ as a bifurcation parameter to demonstrate the existence and stability of natural waves; stability is determined by numerically solving for the zero set of the Evans function, constructed in section 4.2. It is found that the larger, faster wave is stable (black), while the smaller, slower wave is unstable (gray).

Stimulus-locked traveling pulses. Numerically solving (3.10) and (3.11) for $I_0 > 0$, we can determine the regions in the (v, I_0)-plane where one or more stimulus-locked waves exist. First, performing a continuation from the pair of natural waves, we generate a corresponding pair of existence tongues with tips at $I_0 = 0$. These are illustrated in Figure 3.2 with the left-hand (right-hand) tongue emerging from the unstable (stable) natural wave. We then note that the left-hand tongue includes

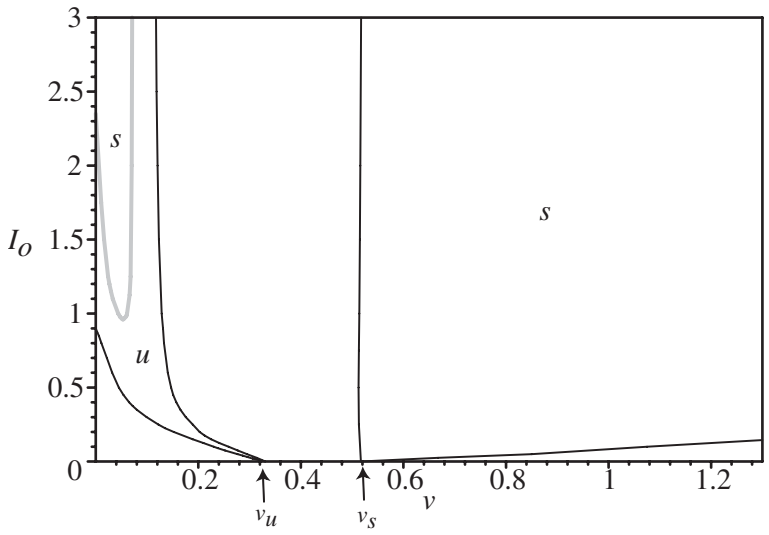

FIG. 3.2. *Regions of existence of the stimulus-locked traveling pulses in the* (v, I_0)*-plane for* $\sigma = 1.0$*,* $\kappa = 0.3$*,* $\epsilon = 0.03$*, and* $\beta = 2.5$*. The left and right regions form tongues that issue from the unstable* v_u *and stable* v_s *natural traveling pulses, respectively. The Hopf curve within the left-hand tongue is shown in gray. Stationary pulses correspond to the intersection of the tongue and the line* $v = 0$*.*

stationary pulses at $v = 0$. In previous work we have shown how a stationary unimodal input can generate a stable stationary pulse that bifurcates to a stable breather via a Hopf bifurcation as the input amplitude is reduced [5, 13]. In section 4 we construct the associated Evans function for traveling pulses within the tongue regions and use this to determine the stability of stimulus-locked pulses. We find that there is a Hopf curve within the left-hand tongue that is a continuation of the Hopf bifurcation point for stationary pulses ($v = 0$); this is shown in Figure 3.2 by the gray curve. Above the Hopf curve the pulse is stable, while it is unstable below. On the other hand the pulse within the right-hand tongue is always stable. Finally, note that there also exist additional stimulus-locked pulse solutions in certain subregions inside as well as outside of the tongues; however, these are found to be always unstable.

4. Stability of the stimulus-locked traveling pulse. We begin by analyzing the resolvent and the spectrum of the operator associated with the linearization of the vector system (1.2) about the general stimulus-locked traveling pulse constructed in section 3.1. This analysis indicates that potential instabilities arise only due to the behavior of eigenvalues, which can be determined by calculation of the zero set of the Evans function. We then present the explicit construction of the Evans function for the stimulus-locked traveling pulse in the particular case of the exponential weight distribution, and calculate the zero sets of this Evans function for the pulse existence tongues shown in Figure 3.2, thereby determining their stability.

4.1. Spectral analysis of the linearized operator. Consider the evolution of small smooth perturbations of the stimulus-locked traveling pulse with stationary form (U, Q),

$$u = U + \bar{\varphi},$$
$$q = Q + \bar{\psi}.$$

Substituting into the system expressed in traveling wave coordinates and linearizing, we find that the perturbations, to first order, satisfy

$$\frac{\partial \bar{\varphi}}{\partial t} - v\frac{\partial \bar{\varphi}}{\partial \xi} + \bar{\varphi} + \beta\bar{\psi} = \int_{\mathbb{R}} w(\xi-\eta)H'(U(\eta)-\kappa)\bar{\varphi}(\eta)d\eta, \tag{4.1}$$

$$\frac{\partial \bar{\psi}}{\partial t} - v\frac{\partial \bar{\psi}}{\partial \xi} - \epsilon\bar{\varphi} + \epsilon\bar{\psi} = 0. \tag{4.2}$$

Separating variables,

$$\begin{pmatrix} \bar{\varphi}(\xi,t) \\ \bar{\psi}(\xi,t) \end{pmatrix} = \begin{pmatrix} \varphi(\xi) \\ \psi(\xi) \end{pmatrix} e^{\lambda t}, \tag{4.3}$$

the spatial components $\varphi, \psi \in \mathcal{C}^1(\mathbb{R},\mathbb{C})$ satisfy the spectral problem

$$(\mathcal{L}+\mathcal{N}_s)\begin{pmatrix} \varphi \\ \psi \end{pmatrix} = \lambda\begin{pmatrix} \varphi \\ \psi \end{pmatrix}, \tag{4.4}$$

where

$$\mathcal{L} = v\frac{\partial}{\partial \xi} - \mathcal{A}, \qquad \mathcal{A} = \begin{bmatrix} 1 & \beta \\ -\epsilon & \epsilon \end{bmatrix}, \tag{4.5}$$

$$\mathcal{N}_s\begin{pmatrix} \varphi \\ \psi \end{pmatrix} = \begin{pmatrix} \frac{w(\xi-\xi_1)}{|U'(\xi_1)|}\,\varphi(\xi_1) + \frac{w(\xi-\xi_2)}{|U'(\xi_2)|}\,\varphi(\xi_2) \\ 0 \end{pmatrix}. \tag{4.6}$$

Resolvent and the point spectrum. Letting $\mathbf{z} = (\varphi,\psi)^T$, we seek to construct a bounded inverse by solving

$$(\mathcal{L}+\mathcal{N}_s-\lambda)\mathbf{z} = -\mathbf{f},$$

where $\mathbf{f} = (f_1,f_2)^T$ and $f_1, f_2 \in \mathcal{C}^0(\mathbb{R},\mathbb{C})$. Following the variation of parameters approach of Zhang [42], we find that the linearly independent solutions of the homogeneous problem $(\mathcal{L}-\lambda)\phi = 0$ are

$$\Phi_+(\xi,\lambda) = \begin{pmatrix} \beta \\ m_+ - 1 \end{pmatrix} e^{\left(\frac{\lambda+m_+}{v}\right)\xi},$$

$$\Phi_-(\xi,\lambda) = \begin{pmatrix} \beta \\ m_- - 1 \end{pmatrix} e^{\left(\frac{\lambda+m_-}{v}\right)\xi},$$

in which case we set

$$\mathbf{z}(\xi) = \Big[\Phi_+\Big|\Phi_-\Big]\begin{pmatrix} \bar{a}(\xi) \\ \bar{b}(\xi) \end{pmatrix}.$$

Subsequently, the coefficient functions are determined according to

$$\Big[\Phi_+\Big|\Phi_-\Big]\frac{\partial}{\partial \xi}\begin{pmatrix} \bar{a} \\ \bar{b} \end{pmatrix} = -\frac{1}{v}\Big(\mathcal{N}_s\mathbf{z}+\mathbf{f}\Big). \tag{4.7}$$

Inversion of $[\Phi_+|\Phi_-]$ leads to

$$\frac{\partial}{\partial \xi}\begin{pmatrix} \bar{a} \\ \bar{b} \end{pmatrix} = -\frac{1}{v\beta(m_+-m_-)}\Big[\Psi_+\Big|\Psi_-\Big]^T\Big(\mathcal{N}_s\mathbf{z}+\mathbf{f}\Big), \tag{4.8}$$

where

$$\Psi_+(\xi,\lambda) = \begin{pmatrix} 1-m_- \\ \beta \end{pmatrix} e^{-\left(\frac{\lambda+m_+}{v}\right)\xi},$$
$$\Psi_-(\xi,\lambda) = -\begin{pmatrix} 1-m_+ \\ \beta \end{pmatrix} e^{-\left(\frac{\lambda+m_-}{v}\right)\xi}.$$

For $\mathcal{R}e(\lambda) > -m_-$, we integrate over $[\xi,\infty)$ to obtain

$$\begin{pmatrix} \bar{a}(\xi) \\ \bar{b}(\xi) \end{pmatrix} = \begin{pmatrix} \bar{a}_\infty \\ \bar{b}_\infty \end{pmatrix} + \frac{1}{v\beta(m_+ - m_-)} \int_\xi^\infty \Big[\Psi_+\big|\Psi_-\Big]^T \big(\mathcal{N}_s\mathbf{z} + \mathbf{f}\big) d\eta,$$

where $\bar{a}_\infty, \bar{b}_\infty$ denote the values of $a(\xi), b(\xi)$ as $\xi \longrightarrow \infty$. Thus

$$\mathbf{z}(\xi) = \Big[\Phi_+\big|\Phi_-\Big] \begin{pmatrix} \bar{a}_\infty \\ \bar{b}_\infty \end{pmatrix} + \frac{1}{v\beta(m_+ - m_-)} \Big[\Phi_+\big|\Phi_-\Big] \int_\xi^\infty \Big[\Psi_+\big|\Psi_-\Big]^T \big(\mathcal{N}_s\mathbf{z} + \mathbf{f}\big) d\eta.$$

As we shall discuss, the integral term is bounded for all ξ, and, consequently, for a bounded solution to exist, we must require that $\bar{a}_\infty = \bar{b}_\infty = 0$. Thus

$$\mathbf{z}(\xi) = \frac{1}{v\beta(m_+ - m_-)} \Big[\Phi_+\big|\Phi_-\Big] \int_\xi^\infty \Big[\Psi_+\big|\Psi_-\Big]^T \big(\mathcal{N}_s\mathbf{z} + \mathbf{f}\big) d\eta,$$

which can be rewritten as

$$\begin{pmatrix} \varphi(\xi) \\ \psi(\xi) \end{pmatrix} - \Lambda_1(\lambda,\xi) \begin{pmatrix} \varphi(\xi_1) \\ 0 \end{pmatrix} - \Lambda_2(\lambda,\xi) \begin{pmatrix} \varphi(\xi_2) \\ 0 \end{pmatrix} = \mathcal{H}(\xi), \tag{4.9}$$

where

$$\Lambda_i(\lambda,\xi) = \frac{1}{v\beta(m_+ - m_-)} \Big[\Phi_+\big|\Phi_-\Big] \int_\xi^\infty \Big[\Psi_+\big|\Psi_-\Big]^T \frac{w(\eta-\xi_i)}{|U'(\xi_i)|}\, d\eta,$$
$$\mathcal{H}(\xi) = \frac{1}{v\beta(m_+ - m_-)} \Big[\Phi_+\big|\Phi_-\Big] \int_\xi^\infty \Big[\Psi_+\big|\Psi_-\Big]^T \mathbf{f}(\eta)\, d\eta.$$

Elements of Λ_i and $\mathcal{H}$ are finite sums of terms of the forms

$$\int_\xi^\infty e^{\left(\frac{\lambda+m_\pm}{v}\right)(\xi-\eta)} w(\eta-\xi_i) d\eta, \qquad \int_\xi^\infty e^{\left(\frac{\lambda+m_\pm}{v}\right)(\xi-\eta)} f_i(\eta) d\eta.$$

Using the Hölder inequality, it is straightforward to show that these terms, and hence Λ_i and $\mathcal{H}$, are bounded for all $\xi \in \mathbb{R}$ and for all $f_i \in \mathcal{C}^0(\mathbb{R},\mathbb{C})$. Now we must determine the conditions under which (4.9) has a unique solution. Since the solution $\mathbf{z}(\xi)$ is determined completely by the restrictions $\mathbf{z}(\xi_1)$ and $\mathbf{z}(\xi_2)$, we obtain the following finite-dimensional system by substituting $\xi = \xi_1, \xi_2$ into (4.9):

$$\Big(\mathbf{I} - \Delta(\lambda)\Big) \begin{pmatrix} \varphi(\xi_1) \\ \varphi(\xi_2) \end{pmatrix} = \begin{pmatrix} \mathcal{H}_1(\xi_1) \\ \mathcal{H}_1(\xi_2) \end{pmatrix},$$

where $\mathcal{H} = (\mathcal{H}_1, \mathcal{H}_2)^T$, $\bar{\Lambda}_i(\lambda,\xi) = (\,1\ 0\,)\ \Lambda_i(\lambda,\xi)\ (\,1\ 0\,)^T$, and

$$\Delta(\lambda,\xi_1,\xi_2) = \begin{pmatrix} \bar{\Lambda}_1(\lambda,\xi_1) & \bar{\Lambda}_2(\lambda,\xi_1) \\ \bar{\Lambda}_1(\lambda,\xi_2) & \bar{\Lambda}_2(\lambda,\xi_2) \end{pmatrix}.$$

This system has a unique solution if and only if $\mathbf{det}(\mathbf{I}-\Delta(\lambda))\neq 0$, resulting in a bounded inverse defined on all of $\mathcal{C}^0(\mathbb{R},\mathbb{C})\times\mathcal{C}^0(\mathbb{R},\mathbb{C})$. All such λ are elements of the resolvent set. Conversely, we cannot invert the operator for λ such that

$$\mathbf{det}\big(\mathbf{I}-\Delta(\lambda,\xi_1,\xi_2)\big)=0,$$

in which case

$$(\mathcal{L}+\mathcal{N}_s-\lambda)\mathbf{z}=0$$

has nontrivial solutions and λ is an element of the point spectrum. As in the scalar front case, the function

$$\mathcal{E}(\lambda,\xi_1,\xi_2)=\mathbf{det}\big(\mathbf{I}-\Delta(\lambda,\xi_1,\xi_2)\big),\qquad \mathcal{R}e(\lambda)>-m_- \tag{4.10}$$

identifies eigenvalues with its zero set, indicating that $\mathcal{E}$ is an Evans function for the set for which $\mathcal{R}e(\lambda)>-m_-$. In a similar fashion, a resolvent and an Evans function can be defined on the set for which $\mathcal{R}e(\lambda)<-m_+$; however, we do not pursue the explicit construction, as it does not reflect an instability of the stimulus-locked wave.

Continuous spectrum. Using arguments similar to those of the case of the scalar equation, it can be shown that the operator $\mathcal{N}_s:\mathcal{C}^1(\mathbb{R},\mathbb{C})\times\mathcal{C}^1(\mathbb{R},\mathbb{C})\longrightarrow\mathcal{C}^0(\mathbb{R},\mathbb{C})\times\mathcal{C}^0(\mathbb{R},\mathbb{C})$ is compact. Again this implies that the essential spectrum of $\mathcal{L}+\mathcal{N}_s$ is identical to that of $\mathcal{L}$. In the case of the vector operator $\mathcal{L}$, the continuous spectrum is the union of the disjoint sets of $\lambda=-m_\pm+iv\rho$, where $\rho\in\mathbb{R}$. To see this, assume such λ and consider the sequence of functions $\phi_n^\pm\in\mathcal{C}^1(\mathbb{R},\mathbb{C})\times\mathcal{C}^1(\mathbb{R},\mathbb{C})$, where n is a positive integer; $\mathcal{Y}_\pm$ are the eigenvectors of the matrix $\mathcal{A}$ defined in (4.5), corresponding to the eigenvalues $m_\pm$; and

$$\phi_n^\pm(\xi)=e^{i\rho\xi}\big(1-e^{-\xi^2/2n^2}\big)\mathcal{Y}_\pm.$$

If $\mathcal{Y}_\pm$ are normalized to unity, then $\big\|\phi_n^\pm\big\|_\infty=1$ for all n; however,

$$\Big\|\mathcal{L}\phi_n^\pm\Big\|=\frac{v}{n^2}\Big\|\xi e^{-\frac{\xi^2}{2n^2}}\Big\|\longrightarrow 0\qquad\text{as}\quad n\longrightarrow\infty.$$

Hence, $(\mathcal{L}-\lambda)^{-1}$ is unbounded, and λ is a member of the continuous spectrum of $\mathcal{L}+\mathcal{N}_s$.

Residual spectrum. To complete the characterization of the spectrum, we demonstrate that the set $\{\lambda\in\mathbb{C}:\mathcal{R}e(\lambda)\in(-m_+,-m_-)\}$ defines the residual spectrum of $\mathcal{L}+\mathcal{N}_s$. We must show that for such λ there exists a bounded inverse whose domain is not dense in $\mathcal{C}^0(\mathbb{R},\mathbb{C})\times\mathcal{C}^0(\mathbb{R},\mathbb{C})$. Consider our previous construction of the inverse operator $(\mathcal{L}+\mathcal{N}_s-\lambda)^{-1}$. Since we need calculate only the residual spectrum of $\mathcal{L}$, we integrate (4.8) over $[c,d]$, neglecting $\mathcal{N}_s$, to obtain

$$\begin{pmatrix}\bar a(d)\\ \bar b(d)\end{pmatrix}-\begin{pmatrix}\bar a(c)\\ \bar b(c)\end{pmatrix}=-\frac{1}{v\beta(m_+-m_-)}\int_c^d\Big[\Psi_+\big|\Psi_-\Big]^T f(\eta)d\eta.$$

There are only two cases to consider. First, taking $c=\xi$ and $d=\infty$, we examine the integral term of $\mathbf{z}(\xi)$, components of which have the form

$$\int_\xi^\infty e^{\left(\frac{\lambda+m_\pm}{v}\right)(\xi-\eta)}\Big[(1-m_\mp)f_1(\eta)+\beta f_2(\eta)\Big]d\eta.$$

Since $\lambda + m_- < 0$ and $v > 0$, all components are bounded, and hence $\mathcal{L} + \mathcal{N}_s - \lambda$ is bounded only if f either decays sufficiently fast such that

$$\int_\xi^\infty e^{\left(\frac{\lambda+m_+}{v}\right)(\xi-\eta)}\Big[(1-m_-)f_1(\eta)+\beta f_2(\eta)\Big]d\eta < \infty, \qquad \xi \in \mathbb{R},$$

or satisfies $(1-m_-)f_1(\eta)+\beta f_2(\eta) = 0$ for all η. Similarly, for $c = -\infty$ and $d = \xi$, we must require that

$$\int_{-\infty}^\xi e^{\left(\frac{\lambda+m_-}{v}\right)(\xi-\eta)}\Big[(1-m_+)f_1(\eta)+\beta f_2(\eta)\Big]d\eta < \infty, \qquad \xi \in \mathbb{R},$$

or $(1-m_+)f_1(\eta)+\beta f_2(\eta) = 0$ for all η. Since the union of all such f is not dense in $\mathcal{C}^0(\mathbb{R},\mathbb{C}) \times \mathcal{C}^0(\mathbb{R},\mathbb{C})$, we conclude that λ lies in the residual spectrum.

4.2. Evans function for stimulus-locked traveling pulses. The following gives the explicit construction of the Evans function for stimulus-locked waves in the case of a Gaussian input, Heaviside firing rate function, and exponential weight distribution. Note that this includes natural waves where $I_0 = 0$. After a lengthy calculation,

$$\begin{aligned}\mathcal{E}(\lambda,\xi_1,\xi_2) &= \mathbf{det}\big(\mathbf{I}-\Delta(\lambda,\xi_1,\xi_2)\big) \qquad\qquad \Re e(\lambda) > -m_-\\ &= \left(1-\frac{\Theta_+(\lambda)}{\big|U'(\xi_1)\big|}\right)\left(1-\frac{\Theta_+(\lambda)}{\big|U'(\xi_2)\big|}\right) - \frac{\Theta_+(\lambda)\Gamma(\lambda)}{\big|U'(\xi_1)U'(\xi_2)\big|}e^{(\xi_1-\xi_2)},\end{aligned} \tag{4.11}$$

where

$$\begin{aligned}\Gamma_\pm(\lambda) &= \frac{(1-m_\mp)v}{(m_+-m_-)(v^2-(\lambda+m_\pm)^2)},\\ \Theta_\pm(\lambda) &= \frac{1}{2(m_+-m_-)}\left(\frac{1-m_-}{\lambda+m_+\pm v}-\frac{1-m_+}{\lambda+m_-\pm v}\right),\\ \Gamma(\lambda) &= \Theta_-(\lambda)e^{(\xi_1-\xi_2)}+\Gamma_+(\lambda)e^{\left(\frac{\lambda+m_+}{v}\right)(\xi_1-\xi_2)}-\Gamma_-(\lambda)e^{\left(\frac{\lambda+m_-}{v}\right)(\xi_1-\xi_2)}.\end{aligned} \tag{4.12}$$

Since the zero set of the Evans function (4.11) comprises solutions of a transcendental equation, we solve for the eigenvalues numerically by finding the intersection points of the zero sets of the real and complex parts of the Evans function. This leads to the stability results shown in Figure 3.2, namely, that pulses within the right-hand tongue are stable whereas pulses within the left-hand tongue are stable only if they lie inside the region enclosed by the Hopf curve. An example of a zero set construction is shown in Figure 4.1 for fixed I_0 and various values of v.

Linear stability of the traveling pulse solution is characterized by all eigenvalues of the linearization having negative real part, with the possible exception that $\lambda = 0$ is a simple eigenvalue. Moreover, Hopf bifurcations may be identified by a pair of complex eigenvalues crossing the imaginary axis from the left-half plane. It has been found in many infinite-dimensional dynamical systems, such as semilinear parabolic equations, that the criterion for a Hopf bifurcation carries over from ordinary differential equations. Although smoothness properties of the flow are required for its proof using invariant manifold theory, the result is *essentially* based on the behavior of eigenvalues of the linearized operator [26]. We shall assume this and use numerical

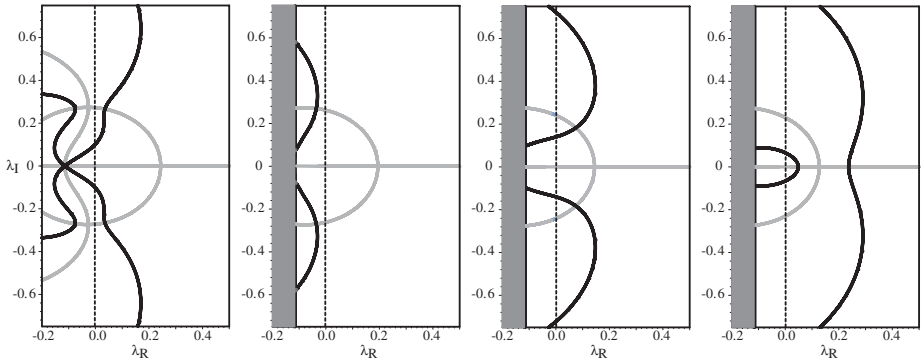

(a) $v = 0.0$ (b) $v = 0.05$ (c) $v = 0.1$ (d) $v = 0.1175$

FIG. 4.1. *Graphs of the zero sets of the real (dark curves) and imaginary (light curves) parts of the Evans functions for* $I_0 = 2.0$ *and a sequence of stimulus speeds* v*; intersection points indicate eigenvalues. Note that the horizontal gray line is part of the zero set of the imaginary part. The vertical shaded region* $\mathcal{R}e(\lambda) \leq -m_-$ *indicates the essential spectrum. This sequence of plots indicates that two Hopf bifurcation points occur, thus defining the boundary of the stable region within the left tongue depicted in Figure* 3.2. *Case* (a) *is associated with the existence of a stable stationary breather, case* (b) *with a stable traveling pulse, and cases* (c) *and* (d) *with a traveling emitter. See text for more details.*

simulations, as discussed in the following section, to explore the behavior of the model near these bifurcation points. Note, for $I_0 > 0$, $\lambda = 0$ is not an eigenvalue and does not complicate the eigenvalue criteria of the standard Hopf bifurcation theorem, as would be the case with natural waves.

4.3. Numerical simulations. In this section we explore the behavior of the vector system (1.2) in all regions of the (v, I_0)-plane shown in Figure 3.2. In particular, we describe the various types of solutions that emerge beyond the Hopf bifurcation curve, as well as beyond the existence tongues.

For parameter values supporting natural traveling waves, and in the absence of an input ($I_0 = 0$), an initial sufficiently large local displacement of the activity u from rest induces a locally excited region of activity, which rapidly develops into a pair of diverging natural traveling pulses, as in the reaction diffusion analogue. Similarly, for parameter values supporting stable stimulus-locked waves in the presence of an input ($I_0 > 0$), an initial displacement of u near the input (or no initial displacement in the case of sufficiently large input strength I_0) rapidly approaches the stable traveling pulse. For certain speeds v the initial transient can generate an additional single or pair of traveling waves that propagate away from the input. As expected, the speed and width of the stimulus-locked traveling pulse closely match those of the theory.

Interestingly, for the parameter values in Figure 3.2, numerical simulations suggest that the left-hand branch of the Hopf curve (gray) corresponds to a supercritical bifurcation, while the right-hand branch is subcritical without a sharp transition to a breathing pulse. We first characterize the nature of solutions obtained by crossing the subcritical branch of the Hopf curve. We find a region of activity moving with the input whose right boundary oscillates with increasing amplitude. After a critical point, the system emits a natural traveling pulse, whose speed is faster than that of the input, as shown in Figure 4.2. The region between the one excited by the

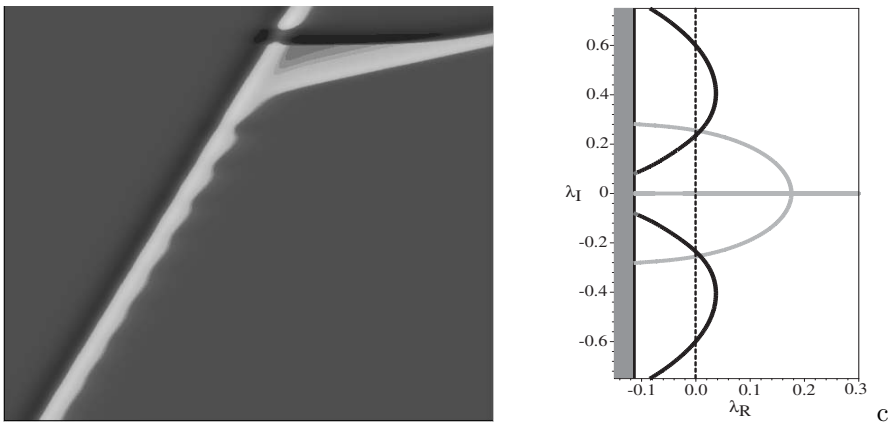

(a) (b)

FIG. 4.2. *Instability of the stimulus-locked traveling pulse in the presence of two complex conjugate eigenvalues with positive real part for* $I_0 = 1.0$, $v = 0.07$, $\sigma = 1$, $\kappa = 0.3$, $\epsilon = 0.03$, *and* $\beta = 2.5$. *In this case the bifurcation appears subcritical with the absence of a sharp jump to a stable breathing pulse. Instead, instability manifests itself as a periodic cycling of an initial phase of periodically modulated growth of the active region, followed ultimately by the shedding of a natural traveling pulse.* (a) *Space-time plot showing one cycle of the instability, where the vertical axis represents time and the horizontal axis represents space.* (b) *Graph of the corresponding zero set of the Evans function. The periodic process of shedding or emitting natural traveling pulses becomes more rapid as the real part of the eigenvalue increases.*

input and the new natural wave recovers, and the process repeats periodically. Such solutions we refer to as *pulse-emitters*. The smaller the real part of the eigenvalue, the slower the instability grows and the more time is required for the wave to be emitted. As v is increased, the real part of the eigenvalue grows and the number of oscillations occurring before the shedding of natural waves decreases, until the eigenvalues become real, as illustrated in the figure sequence 4.1(b)–(d), and the pulse rapidly emits natural pulses. This behavior continues until v is increased to the boundary of the right-hand tongue where there is a smooth transition to a stable stimulus-locked pulse.

When the left-hand supercritical branch of the Hopf curve is crossed by reducing I_0 or v, we find a smooth transition to a stimulus-locked traveling breather. In the special case of a stationary stimulus ($v = 0$), reducing I_0 generates a stationary breather, as we have shown previously [5, 13]. The breathing solutions continue to persist in a subregion of the (v, I_0)-plane bounded to the right by the left (supercritical) branch of the Hopf curve in 3.2. As one moves in this subregion away from the left Hopf branch, the amplitude of the oscillations grows. After some point, the breathing solution disappears, and a new type of temporally periodic solution appears, each cycle of which is characterized by one or more breathing pulse oscillations followed by the emission of a pair of natural waves, possibly intermixed with interludes of subthreshold behavior. An example of such a transition is illustrated in Figure 4.3. This type of pulse-emitting solution appears to be part of a family of related responses of the system to a localized input, which also includes the pulse-emitting behavior associated with the region between the subcritical Hopf curve and the stable right

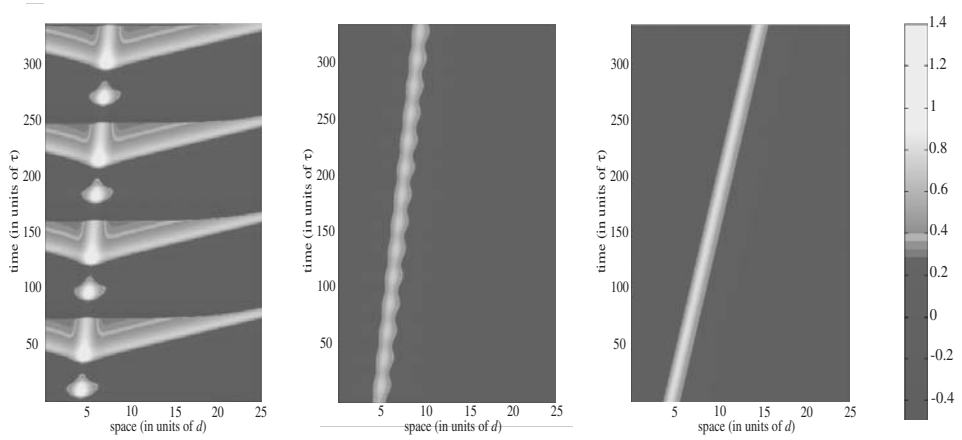

(a) $v = 0.01$ (b) $v = 0.014$ (c) $v = 0.03$

FIG. 4.3. *Sequence of space-time plots for fixed input* $I_0 = 1.5$*, illustrating the transition from pulse emitter, to breather, to stimulus-locked pulse as* v *increases through the supercritical branch of the Hopf curve shown in Figure* 3.2*. Other parameters are* $\epsilon = 0.03$*,* $\kappa = 0.3$*,* $\beta = 2.5, \sigma = 1$*.*

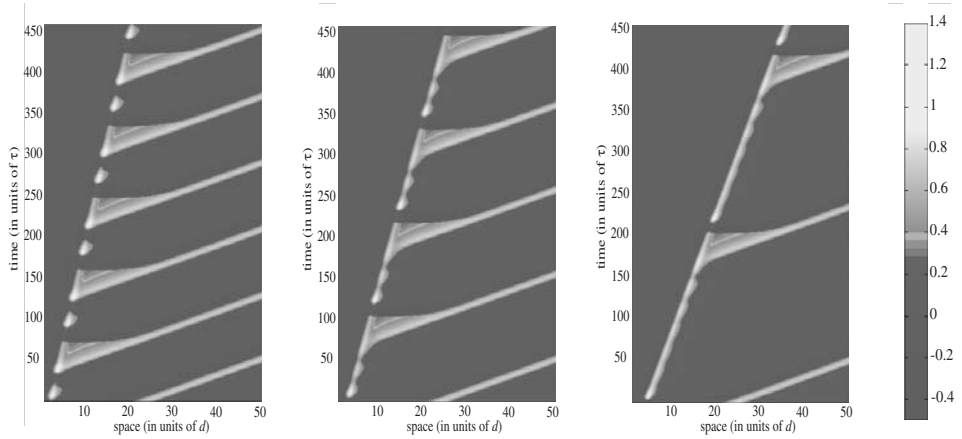

(a) $v = 0.04$ (b) $v = 0.05$ (c) $v = 0.07$

FIG. 4.4. *Transitions between various pulse-emitting solutions for fixed* $I_0 = 0.9$ *as* v *is increased. These solutions exist within the unstable part of the left-hand tongue of Figure* 3.2*, sufficiently below the Hopf curve such that stable breathers no longer exist. Other parameters are* $\epsilon = 0.03$*,* $\kappa = 0.3$*,* $\beta = 2.5$*,* $\sigma = 1$*.*

tongue shown in Figure 3.2. Furthermore, there is a smooth transition of behaviors joining the two regions, as shown in Figure 4.4.

Although the above account applies to the case $\sigma = 1$, most features are valid for more general σ. One main point of difference lends insight into the disappearance of the breather. If we consider stationary pulses for $\sigma = \sqrt{2}$ and explore the evolution of the breathing pulse as we further decrease I_0 beyond the bifurcation point, we find that a secondary bifurcation occurs, giving rise to two modes of breathing rather than

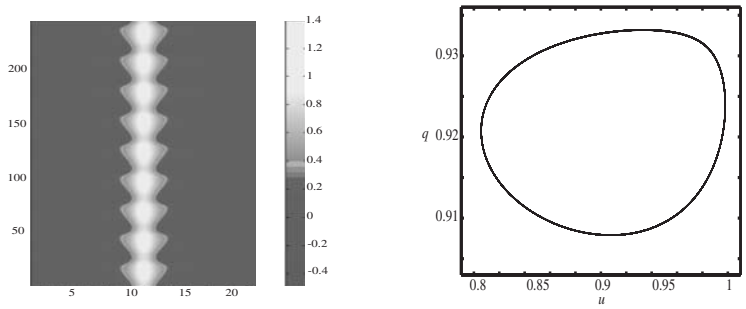

(a) $I_0 = 2.4$

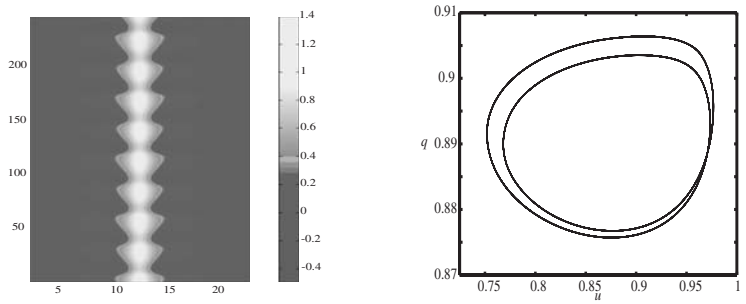

(b) $I_0 = 2.3$

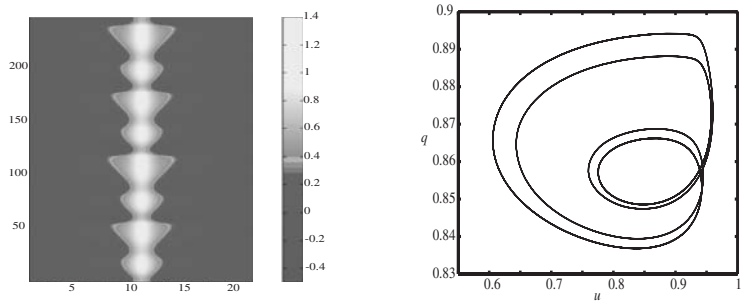

(c) $I_0 = 2.2$

FIG. 4.5. *Sequence of period-doubling bifurcations of a breathing pulse for* $\sigma = \sqrt{2}$. *The left-hand column shows space-time plots for different values of current amplitude beyond the initial Hopf bifurcation point, with an orbit corresponding to the center spatial point plotted in the* (u, q)*-phase plane in the right-hand column; other spatial points are qualitatively similar. Other parameter values are* $\kappa = 0.3$, $\beta = 2.5$, $\epsilon = 0.03$, $v = 0$. *(Note that at higher resolution each loop in* (c) *is actually a pair of closely spaced loops, indicating that it corresponds to the third doubling in the sequence.)*

one. By graphing, in the (u, q)-phase plane, the orbit corresponding to a spatial point at the center of the input, we find that the evolution of the orbit, as I_0 is decreased, strongly resembles that of a period-doubling bifurcation, as shown in Figure 4.5(a)–(b). Decreasing I_0 leads to additional period doublings, as illustrated in Figure 4.5(c). Ultimately, decreasing I_0 leads to behavior similar to that found for $\sigma = 1$. This suggests that for $\sigma = 1$ the first period-doubling bifurcation may be subcritical, and the orbit instead weaves its way around the unstable limit cycle giving rise to the sequence of breathing pulses and emission, as shown in Figure 4.6.

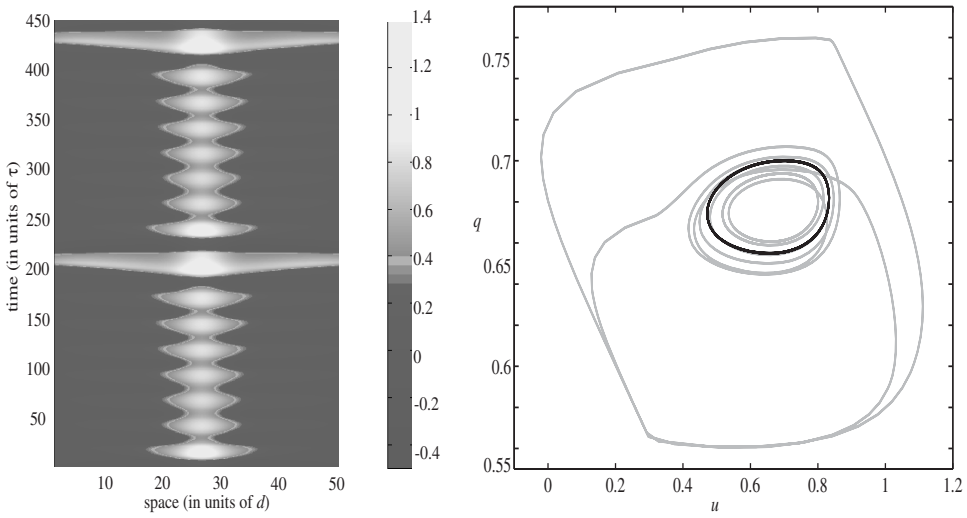

(a) (b)

FIG. 4.6. (a) *Space-time plot of a stationary ($v = 0$) pulse-emitter for $\sigma = 1$, $I_0 = 1.35$, $\kappa = 0.3$, $\beta = 2.5$ and $\epsilon = 0.03$.* (b) *Corresponding phase portrait showing the orbit (gray trajectory) of the center spatial point plotted in the (u, q)-phase plane. Also shown is the corresponding orbit (black trajectory) of the stable breather that exists when $I_0 = 1.4$.*

5. Discussion. In this paper we have shown how to extend the analysis of the existence and stability of pulses arising from a stationary stimulus input to that of a input moving with constant speed. We described the continuation from the unstable/stable pair of natural waves by constructing a corresponding pair of existence tongues emerging from the natural waves at $I_0 = 0$, with the left-hand tongue including stationary pulses at $v = 0$, for a particular choice of parameter values supporting natural waves. We have extended Zhang's analysis of stability of natural waves to that of stimulus-locked waves and numerically evaluated the Evans function to determine eigenvalues away from the singular limit $\epsilon \to 0$. This allowed us to analyze the stability of the existence tongues in the (v, I_0)-plane and show the continuation of the Hopf bifurcation found for stationary pulses. Numerically this Hopf curve was found to have a supercritical branch, from which breathing pulses emerge and a subcritical branch from which no breathing pulse emerges. In general for parameter values that do not support either stimulus-locked pulses or breathers, the system generates more complicated behavior, including the emission of natural traveling waves when such waves exist.

It would be interesting to contrast the type of local inhibition analyzed in this paper, which is primarily due to intrinsic neuronal properties, with that of nonlocal inhibition, arising from the ubiquitous inhibitory populations of neurons found in cortex. From previous work [1, 28], we know that the two-population, excitatory-inhibitory system supports stable stationary pulses which, moreover, can undergo a subcritical Hopf bifurcation. In this case no breathing pulse emerges; however, it is possible that the presence of a localized input is capable of stabilizing such a breathing pulse solution. In addition, it would be interesting to provide a more thorough analysis

of the scalar model considered by Xie and Giese [40], by constructing tongue diagrams and Hopf bifurcation curves and, furthermore, considering the effect of varying the degree of nonlocal inhibition.

From a more general perspective, the analysis presented here and in related work [6, 13] has established that the combined effect of local inhomogeneities and recurrent synaptic interactions can result in nontrivial forms of coherent oscillations and waves. Although we have focused on rather abstract neural field equations, we expect our results to carry over (at least qualitatively) to more biophysically realistic conductance-based models. Indeed, elsewhere we have confirmed the existence of stationary breathers and pulse emitters in the case of a modified Traub model [13]. One of the advantages of studying simplified models is that it can generate predictions regarding how dynamical properties such as wave speed depend on characteristic features of neural tissue. One striking demonstration of this is the recent study of wave propagation in disinhibited cortical slices, where the speed of the wave was controlled by external electric fields, confirming predictions based on homogeneous neural field equations [32]. Our own work predicts that coherent oscillations can be induced by local inhomogeneities. Such inhomogeneities could arise from external stimuli or reflect changes in the excitability of local populations of neurons. The former suggests a network mechanism for stimulus-induced oscillations, which may play an important role in visual processing [17], whereas the latter suggests a network mechanism for generating epileptiform activity.

REFERENCES

[1] S. Amari, *Dynamics of pattern formation in lateral inhibition type neural fields*, Biol. Cybernet., 27 (1977), pp. 77–87.

[2] M. Bode, *Front bifurcations in reaction-diffusion systems with inhomogeneous parameter distributions*, Phys. D, 106 (1997), pp. 270–286.

[3] P. C. Bressloff, *Traveling waves and pulses in a one-dimensional network of excitable integrate-and-fire neurons*, J. Math. Biol., 40 (2000), pp. 169–198.

[4] P. C. Bressloff, *Traveling fronts and wave propagation failure in an inhomogeneous neural network*, Phys. D, 155 (2001), pp. 83–100.

[5] P. C. Bressloff, S. E. Folias, A. Prat, and Y-X. Li, *Oscillatory waves in inhomogeneous neural media*, Phys. Rev. Lett., 91 (2003), 78101.

[6] P. C. Bressloff and S. E. Folias, *Front bifurcations in an excitatory neural network*, SIAM J. Appl. Math., 65 (2004), pp. 131–151.

[7] R. D. Chervin, P. A. Pierce, and B. W. Connors, *Periodicity and directionality in the propagation of epileptiform discharges across neocortex*, J. Neurophysiol., 60 (1988), pp. 1695–1713.

[8] S. Coombes and M. R. Owen, *Evans functions for integral neural field equations with Heaviside firing rate function*, SIAM J. Appl. Dynam. Syst., 3 (2004), pp. 574–600.

[9] G. B. Ermentrout and J. B. Mcleod, *Existence and uniqueness of travelling waves for a neural network*, Proc. Roy. Soc. Edinburgh A, 123 (1993), pp. 461–478.

[10] J. W. Evans, *Nerve axon equations:* IV. *The stable and unstable impulse*, Indiana Univ. Math. J., 24 (1975), pp. 1169–1190.

[11] J. W. Evans and J. Feroe, *Local stability theory of the nerve impulse*, Math. Biosci., 37 (1977), pp. 23–50.

[12] R. FitzHugh, *Impulses and physiological states in theoretical models of nerve membrane*, Biophys. J., 1 (1961), pp. 445–466.

[13] S. E. Folias and P. C. Bressloff, *Breathing pulses in an excitatory neural network*, SIAM J. Appl. Dynam. Syst., 3 (2004), pp. 378–407.

[14] D. Golomb and Y. Amitai, *Propagating neuronal discharges in neocortical slices: Computational and experimental study*, J. Neurophysiol., 78 (1997), pp. 1199–1211.

[15] D. Golomb and G. B. Ermentrout, *Continuous and lurching traveling pulses in neuronal networks with delay and spatially decaying connectivity*, Proc. Natl. Acad. Sci. USA, 96 (1999), pp. 13480–13485.

[16] D. Golomb and G. B. Ermentrout, *Bistability in pulse propagation in networks of excitatory and inhibitory populations*, Phys. Rev. Lett., 86 (2001), pp. 4179–4182.
[17] C. M. Gray, *Synchronous oscillations in neuronal systems: Mechanisms and functions*, J. Comput. Neurosci., 1 (1994), pp. 11–38.
[18] A. Hagberg and E. Meron, *Pattern formation in non-gradient reaction-diffusion systems: The effects of front bifurcations*, Nonlinearity, 7 (1994), pp. 805–835.
[19] A. Hagberg, E. Meron, I. Rubinstein, and B. Zaltzman, *Controlling domain patterns far from equilibrium*, Phys. Rev. Lett., 76 (1996), pp. 427–430.
[20] A. L. Hodgkin and A. F. Huxley, *A quantitative description of membrane current and its application to conduction and excitation in nerve*, J. Physiol., 117 (1952), pp. 500–544.
[21] M. A. P. Idiart and L. F. Abbot, *Propagation of excitation in neural network models*, Network, 4 (1993), pp. 285–294.
[22] C. K. R. T. Jones, *Stability of the traveling wave solution of the FitzHugh–Nagumo system*, Trans. Amer. Math. Soc., 286 (1984), pp. 431–469.
[23] T. Kapitula, N. Kutz, and B. Sandstede, *The Evans function for nonlocal equations*, Indiana Univ. Math. J., 53 (2004), pp. 1095–1126.
[24] T. Kato, *Perturbation Theory for Linear Operators*, Springer-Verlag, New York, 1966.
[25] R. Maex and G. A. Orban, *Model circuit of spiking neurons generating direction selectivity in simple cells*, J. Neurophysiol., 75 (1996), pp. 1515–1545.
[26] J. Marsden and M. McCracken, *Hopf Bifurcation and Its Applications*, Appl. Math. Sci. 10, Springer-Verlag, New York, 1976.
[27] D. J. Pinto and G. B. Ermentrout, *Spatially structured activity in synaptically coupled neuronal networks:* I. *Traveling fronts and pulses*, SIAM J. Appl. Math., 62 (2001), pp. 206–225.
[28] D. J. Pinto and G. B. Ermentrout, *Spatially structured activity in synaptically coupled neuronal networks:* II. *Lateral inhibition and standing pulses*, SIAM J. Appl. Math, 62 (2001), pp. 226–243.
[29] D. Pinto, S. L. Patrick, W. C. Huang, and B. W. Connors, *The fine structure of epileptiform activity in neocortex in vitro*, submitted.
[30] D. Pinto, S. L. Patrick, W. C. Huang, and B. W. Connors, *Mechanisms of initiation, propagation, and termination of epileptiform activity in neocortex in vitro*, submitted.
[31] A. Prat and Y.-X. Li, *Stability of front solution in inhomogeneous media*, Phys. D, 186 (2003), pp. 50–68.
[32] K. A. Richardson, S. J. Schiff, and B. J. Gluckman, *Control of traveling waves in the mammalian cortex*, Phys. Rev. Lett., 94 (2005), paper 028103.
[33] J. Rinzel and J. P. Keener, *Hopf bifurcation to repetitive activity in nerve*, SIAM J. Appl. Math., 43 (1983), pp. 907–922.
[34] J. Rubin, *A nonlocal eigenvalue problem for the stability of a traveling wave in a neuronal medium*, Discrete Contin. Dynam. Syst. A, 4 (2004), pp. 925–940.
[35] B. Sandstede, *Stability of travelling waves*, in Handbook of Dynamical Systems II, B. Fiedler, ed., North–Holland, Amsterdam, 2002, pp. 983–1055.
[36] P. Schutz, M. Bode, and H.-G.- Purwins, *Bifurcations of front dynamics in a reaction-diffusion equation system with spatial inhomogeneities*, Phys. D, 82 (1995), pp. 382–397.
[37] H. Suarez, C. Koch, and R. Douglas, *Modeling direction selectivity of simple cells in striate visual cortex within the framework of the canonical microcircuit*, J. Neurosci., 15 (1995), pp. 6700–6719.
[38] H. R. Wilson and J. D. Cowan, *A mathematical theory of the functional dynamics of cortical and thalamic nervous tissue*, Kybernetik, 13 (1973), pp. 55–80.
[39] J.-Y. Wu, L. Guan, and Y. Tsau, *Propagating activation during oscillations and evoked responses in neocortical slices*, J. Neurosci., 19 (2001), pp. 5005–5015.
[40] X. Xie and M. Giese, *Nonlinear dynamics of direction-selective recurrent neural media*, Phys. Rev. E, 65 (2002), paper 051904.
[41] K. Yosida, *Functional Analysis*, Springer-Verlag, New York, 1968.
[42] L. Zhang, *On stability of traveling wave solutions in synaptically coupled neuronal networks*, Differential Integral Equations, 16 (2003), pp. 513–536.
[43] L. Zhang, *Existence, uniqueness, and exponential stability of traveling wave solutions of some integral differential equations arising from neuronal networks*, J. Differential Equations, 197 (2004), pp. 162–196.